I&EC research
Industrial & Engineering Chemistry Research

pubs.acs.org/IECR

Article

Variable-Area Sensor Permits Near-Continuous Multipoint Measurements of Aqueous Biological and Chemical Analytes

Published as part of Industrial & Engineering Chemistry Research special issue "Inverse Design of Materials and Processes for Separations".

Liza R. White, Jordan N. Miner, Luke D. McKinney, Lindsay E. Pierce, Anna Folley, Ariel Larrabee, Lea Scrapchansky, Wyatt Fessler, Manisha Choudhary, Manoj Kamalanathan, Ramin Pouria, Saman Zare, Emma Perry, Sheila Edalatpour, Onur G. Apul, and Caitlin Howell*

Cite This: *Ind. Eng. Chem. Res.* 2025, 64, 382−391

Read Online

ACCESS | Metrics & More | Article Recommendations | Supporting Information

ABSTRACT: The timely detection of aqueous analytes is critical to decision-makers in agriculture, industry, and municipalities. However, nearly all aqueous sensor systems rely on single-point measurements, often taken at an instantaneous point in time and in one location, which can limit their ability to detect analytes passing through the aqueous solution at other locations or times. In this work, we present the concept of employing a mass-manufactured nanotextured diffraction surface as a variable-area sensor system capable of providing spectrophotometric information about aqueous analytes across multiple locations over time. We show that by placing the nanotextured surface of the sensor system under or behind a water sample, the water can be scanned by simply changing the location or angle of the light source and detector. We demonstrate the detection and quantification of a variety of aqueous analytes, including visible and ultraviolet (UV)-absorbing dyes, dust particles, and microalgae species, at accuracies similar to those of commercial equipment. A machine-learning algorithm was used to lower the limit of detection of dye from 5 to 3 μg/mL as well as automate the classification of distinct analyte types. These results demonstrate that using a mass-manufactured, textured surface can offer benefits as aqueous sensors, facilitating widely deployable aqueous analyte monitoring in a variety of applications.

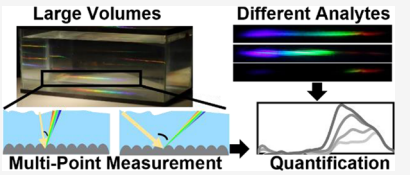

1. INTRODUCTION

Reliable and timely detection of aqueous analytes is essential across agriculture, industry, and municipal life.[1−4] Most often, the presence of chemical and biological species in water is monitored using discrete sampling of relatively small volumes executed by trained professionals, which is laborious, costly, and time-consuming.[5−7] Also, measuring small volumes collected at single points or composites collected over multiple time points can miss critical information if the chemical or biological analyte of interest is either in a different location or passes through the system when active sampling is not occurring.[4−6,8,9] To better facilitate the timely detection of aqueous analytes and more effectively deploy mitigation, remediation, or other intervention strategies, widely deployed sensor systems that can sample aqueous solutions continuously are urgently needed, particularly as pollution of natural source waters reaches increasingly higher levels.[4]

Absorbance spectrophotometry is favored for water analysis as it is well-suited to detect a wide range of aqueous analytes from dyes[10] and pesticides to suspended sediment and microorganisms.[11] Relying on the unique light absorbance and transmission properties of chemical compounds,[12] absorbance spectrophotometers have been used in recent years to identify and determine the concentration of dissolved organic carbon,[13] nitrate and nitrites,[14] total suspended solids,[15] and other aqueous analytes, without the need for tedious preparation steps or harsh reagents.[16] Recognizing the need for broader sampling, focus has recently shifted toward developing spectrophotometers capable of near-continuous monitoring, with fully submersible absorbance spectrophotometers gaining in popularity.[8,17,18] In near-continuous monitoring, a probe is deployed into a strategic location and the data acquired is constrained to the immediate vicinity of the probe.[19] Yet despite these advances, measurements remain spatially and temporally confined to the deployed probe, with costs limiting the number of probes available. This is increasingly true, as more frequent natural disasters result in the loss or destruction of sensor equipment. To achieve truly effective, widespread, and robust monitoring of the aqueous solutions, more inexpensive and easily replaced sensors are needed.[20−22]

Received: July 24, 2024
Revised: November 10, 2024
Accepted: November 15, 2024
Published: November 25, 2024

To the best of our knowledge, a network of widely deployable sensors capable of monitoring arbitrary volumes of water in a near-continuous mode is not presently available. The capacity of a low-cost surface to act as a sensor that can be easily deployed and cheaply replaced holds the potential to provide comprehensive insights into the overall composition and dynamics as well as both temporal and spatial variations within water streams. This could be particularly advantageous in heterogeneous water samples or in multiple simultaneous flows where conventional sampling techniques may fail to detect time- or location-dependent changes in the water content. However, such a sensor system would have to be cost-effective to be truly field deployable,[9,23] as there is currently a lack of low-cost solutions for near-continuous detection of water composition.[24−26]

In this work, we demonstrate a method for detecting aqueous analytes by using a mass-produced diffraction surface capable of providing photospectroscopic information. The sensor system uses a variable-area (up to hundreds of meters squared per sensor) commercial diffraction texture, originally created for the fashion industry,[27] that can be cut to a desired size and placed below or behind a volume of water. The diffraction surface can be illuminated by a low-cost LED, penetrating through the aqueous solution and generating a diffraction pattern containing information about the analytes within the solution, which can then be captured by a camera. We demonstrate how multiple points within the aqueous solution can be measured by moving the location of the LED/camera setup as well as changing the angle between the two, allowing for multiple points of measurement within a single volume. The sensor system's near-continuous functionality is shown by identifying shifts in the water composition in 1 s intervals. We tested the system against several environmentally relevant chemical and biological analytes, finding that the diffraction system can detect changes in ultraviolet and visible light, similar to current commercial spectrophotometers. We then compared our system to a commercial turbidimeter, demonstrating the diffraction sensor's ability to detect inorganic suspended matter. Together, our work shows the transformative potential of using mass-manufactured diffraction as a low-cost and variable-area water monitoring system.

2. MATERIALS AND METHODS

2.1. Materials and Chemicals. The chemicals and materials were used as received. The Allura Red, Tartrazine, and Fast Green dyes were purchased from Sigma-Aldrich (Burlington, MA). The 1,9-dimethyl methylene blue, nickel-(II) sulfate hexahydrate, and blunt tip needles were purchased from Sigma-Aldrich. The ISO 12103−1 A2 fine test dust, phosphate-buffered saline (PBS), and 1.52 mm inner diameter polyvinyl chloride tubing were purchased from Fisher Scientific (Waltham, MA). The *Rhodomonas sp.* (CCMP 739) were purchased from the National Center for Marine Algae and Microbiota. The white-light-emitting diode (LED) was purchased from Adafruit Industries (New York, NY) and UV-LED was purchased from EDGELEC (Shenzhen, China). The diffraction surface material Rainbow Coated Ultracast 947,[28] 22.68 kg, 160.02 cm wide roll was donated by Sappi North America (Westbrook, ME). According to the manufacturer, the Rainbow Coated Ultracast 947 consists of a transparent film backing coated with a thin polymer layer containing textured periodic ridges that run the length of the material. The ridges were found to have a height of 250−300 nm and width of 641 ± 17 nm and are separated by spaces of 228 ± 44 nm. The refractive index was found to be 1.59 for the *d* line and 1.60 for the *e* line of the film backing, while for the coating it was measured to be 1.60 (*d* line) and 1.61 (*e* line) (Figure S1).

2.2. Diffraction Surface Sample Preparation and Image Collection. The diffraction surface was prepared for imaging by cleaning with soap and water and cut into a circle with a diameter of 100 mm. The diffraction surface was fixed to a black matte-painted square polystyrene dish. The prepared diffraction surface and white LED light source were placed below the camera (Canon EOS RP, B&H Photo Video, New York, NY). The LED was 15 cm from the diffraction surface at an angle of 120°. The camera was normal to the diffraction surface at a distance of 40 cm. For the absorbance experiments, the camera was set with an aperture of 14, shutter speed of 1/320 s, ISO of 6400, and white balance of 2500 K. For the turbidity experiment, the was set with an aperture of 7.1, shutter speed of 1/250 s, ISO of 6400, and white balance of 2500 K. All images acquired were exported in sRGB jpg format with a resolution of 6240 × 4160 pixels (~355 × 235 mm). During near-continuous image collection, an image was acquired at one frame per s.

2.3. Discrete Aqueous Analyte Addition. A 100 × 15 mm polystyrene Petri dish was placed on the diffraction surface. The Petri dish was filled to a water depth of 3.3 mm. The aqueous analyte was pipetted into the Petri dish, mixed with the tip of the pipet until the mixture appeared homogeneous, and then the same volume was removed to ensure constant water volume throughout the experiment. For discrete additions of aqueous analyte experiments, increments of 20 μL of methylene blue (1 mg/mL) were added to 20 mL of water. For the Allura Red experiments, increments of 20 μL was added in 20 mL of water. For the nickel sulfate experiments, increments of 1 mL of nickel sulfate (0.2 g/mL) were added in 20 mL of water. An image was acquired for every aqueous analyte level, as described above.

2.4. Near-Continuous Aqueous Analyte Addition. A 100 × 15 mm Petri dish was prepared for near-continuous addition of an aqueous analyte by cutting holes into opposite sides of the dish, and blunt tip needles were attached. Inlet and outlet polyvinyl chloride pump tubing were connected to the blunt tip needles. The Petri dish was filled to a water depth of 10 mm. A peristaltic pump (Ismatec, Glattbrugg, Switzerland) was set for dispensing at a rate of 9 mL/min through the inlet tubing and retracted at a rate of 9 mL/min through the outlet tubing to ensure constant water volume throughout the experiment. A 10 mm stir bar was placed into the middle of the Petri dish and set to stir at a low speed, to avoid disturbing the surface of the water. During the first 90 s, 0.1 mg/mL of methylene blue dye was dispensed into the Petri dish. After the first 90 s, Milli-Q water was dispensed into the Petri dish until the water in the Petri container appeared colorless (1910 s).

2.5. Large-Surface Area Sensor Imaging. The diffraction surface was cut to fit a 20-gallon rectangular glass aquarium tank and a 30-gallon circular fiberglass tank with a black poly liner. The diffraction surface was taped to the back of the glass tank and to the inside of the polycarbonate tank. The tanks were filled with tap water to approximately 3/4 from the top. A point-source light was pointed toward the surface, and photos of the diffraction patterns were taken.

2.6. Multipoint Measurements via Angle Modulation. The diffraction surface was prepared on 100 × 15 mm Petri

https://doi.org/10.1021/acs.iecr.4c02774
Ind. Eng. Chem. Res. 2025, 64, 382−391

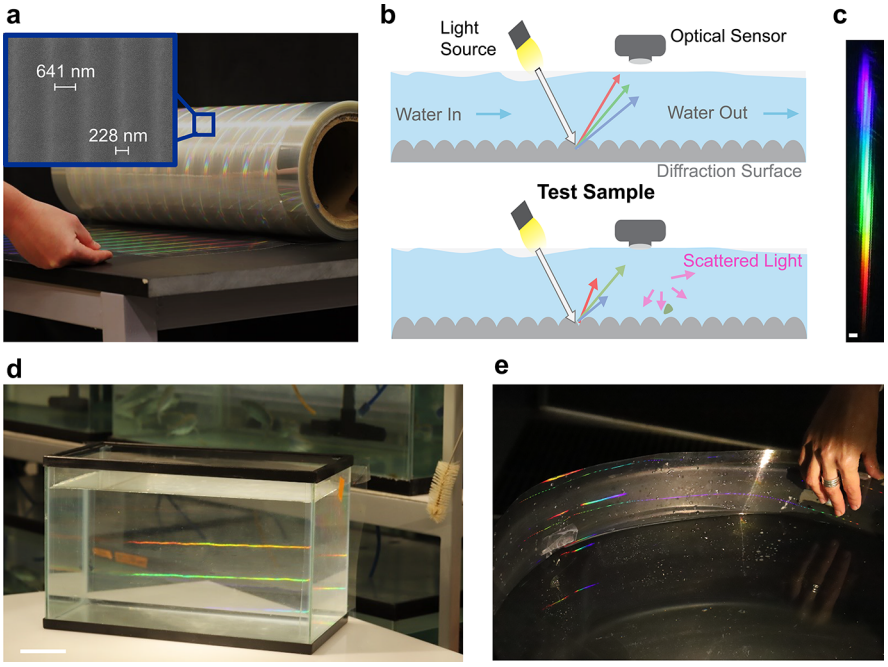

Figure 1. (a) Photograph of the mass-manufactured roll of the diffraction surface texture. A SEM image of the diffraction surface texture is shown in the inset. (b) Schematic of the continuous diffraction surface sensor in both control (clean) conditions and test (containing an aqueous analyte) conditions. (c) Representative image of the clean diffraction pattern. Scale bar: 1 mm. (d) Standard 20 gallon aquarium tank. Scale bar: 30 cm. (e) Pilot-sized aquaculture tank (30 gallon).

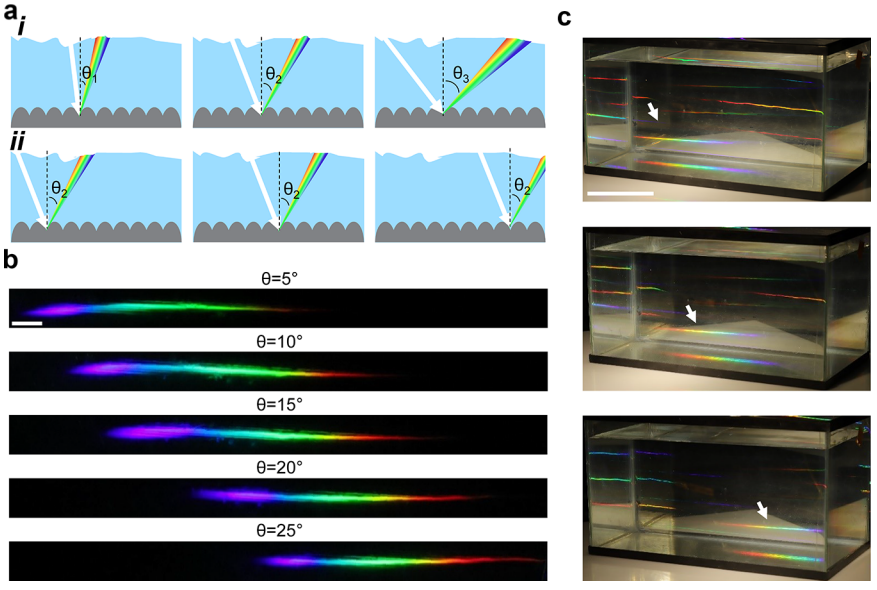

Figure 2. (a) Schematic of the effect of the angle of light on the diffraction pattern location with (*i*) representing angle modulation and (*ii*) detector translation. (b) Representative images of the diffraction pattern at different light angles. Scale bar 5 mm. (c) Diffraction pattern moving across an aquarium tank. Arrow shows the movement of the diffraction pattern through the volume. Scale bar 30 cm.

dish. The Petri dish was filled with deionized water, resulting in a depth of 3.3 mm. A LED light source was positioned above the diffraction surface with a distance normal to the surface of 15 cm. The LED was moved from 5° to 25° in increments of 5° between each image.

2.7. Statistical Analysis. All statistical analysis tests were completed using GraphPad Prism 10. Shapiro–Wilk tests were used to test the sample's normality at the 95% level of significance (α = 0.05). The Kruskal–Wallis test assessed the statistical differences in the peak absorbances for the methylene blue limit of detection samples (n = 5).

3. RESULTS AND DISCUSSION

3.1. Diffraction Surface and Sensor Setup. Our goal was to develop a method for detecting aqueous analytes and turbidity (an aggregate water quality parameter) using a low-cost, mass-manufactured sensor system that could be widely deployed. To accomplish this, we used a mass-manufactured diffraction texture combined with an LED, camera, and image analysis software. The fact that this diffraction texture is currently produced at a massive scale (4,200 m^2/h) could allow for functional sensor components to be easily trans-

https://doi.org/10.1021/acs.iecr.4c02774
Ind. Eng. Chem. Res. 2025, 64, 382–391

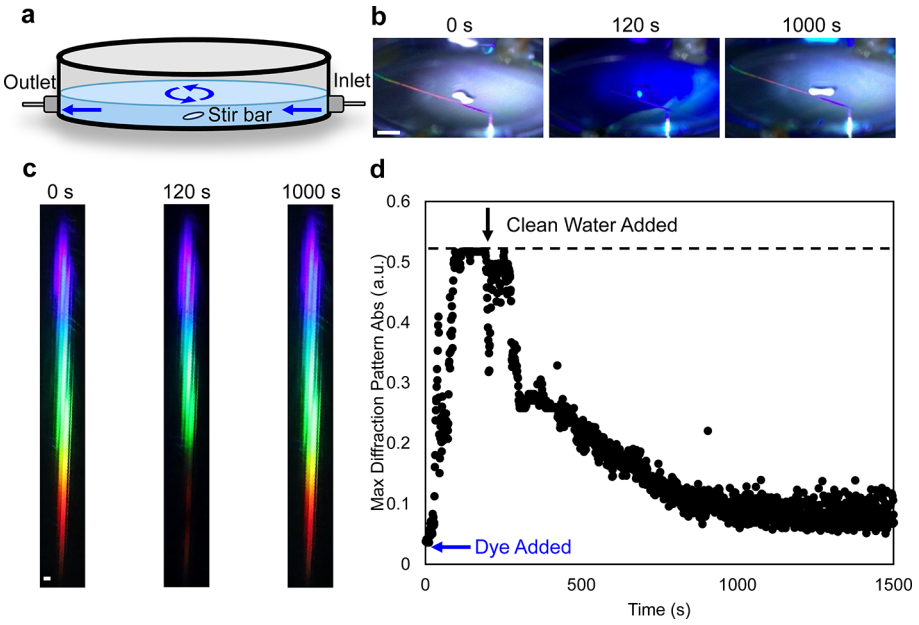

Figure 3. (a) Schematic of experimental design. (b) Representative images of the dye in the water at set time points with a white stir bar facilitating mixing of the fluids. Scale bar 1 cm. (c) Representative images of the diffraction pattern. Scale bar 1 mm. (d) Calculated absorption over time graph of the diffraction pattern with a dashed line to show the max absorbance of the methylene blue dye.

ported, adjusted to a size suitable for a given location, and cheaply replaced upon damage or loss, unlocking new potentials for water widespread monitoring sensor systems. As this diffraction grating material is not fabricated in a cleanroom, the diffraction texture may contain occasional dust particles, divots, or protrusions. As a result, the baseline for the sensor must be set with clean water prior to the measurement of aqueous analytes. Figure 1a shows a roll of the mass-manufactured diffraction surface with an SEM image of the texture on the transparent substrate shown as an inset. To better understand the interactions among the textured coating, transparent material, and light, the refractive index was measured and is shown in Figure S1. The refractive index of the *d* and *e* lines was found to be between 1.59 and 1.60, respectively, for the underlying transparent material and between 1.60 and 1.61, respectively, for the nanotextured coating on top. A schematic of the diffraction sensor system under both control and test conditions is shown in Figure 1b. When an aqueous analyte is present, the particles (depicted in green) absorb the red and blue segments of the visible light spectrum. In contrast, the green segment is refracted and detectable through the optical sensor output. Particle sizes larger than the wavelength of light[29] prompt the dispersion of the light rays across the water medium (Mie scattering), contributing to increased background brightness.[30] The diffraction pattern in clean water conditions with the spectrum of blue, cyan, green, orange, yellow, and red regions that contain no breaks between the colors, as shown in Figure 1c. Additionally, to show the ability to turn any large area into a sensor, we imaged the sensor in two tanks, as shown in Figure 1d,e. The ability of the diffraction sensor to be applied behind the aqueous solution of a standard 20 gal glass aquarium tank is shown in Figure 1d. Figure 1e shows the ability of the diffraction sensor to line a 30 gal industrial water tank used in research and development of aquaculture.

3.2. Multipoint Detection of Aqueous Analytes. The diffraction surface used in this study is currently commercially manufactured in a roll-to-roll process at rates of up 4,200 m^2/h; therefore, in addition to being highly sensitive to incident light angles, it can also be used to cover large areas, enabling the measurement of user-defined portions of the bulk aqueous solution simply by angle modulation (Figure 2a*i*) or detector translation (Figure 2a*ii*). Angle modulation was used to measure the bulk aqueous solution. An LED was set up to move between 5° and 25° in increments of 5°, while the camera remained in a fixed position. Figure 2a shows a schematic of how the incident light angle changes the location of the resulting diffraction pattern. The clean diffraction pattern is shown in Figure 2b. As the incident light angle is changed, the diffraction pattern moves from left to right, measuring different bulk aqueous solutions with every angle change. Figure 2c shows how multipoint measurements could be employed in a glass aquarium tank, as the diffraction pattern, highlighted by a white arrow, moves across the back of the tank with angle modulation. The ability of the diffraction pattern to move to measure the bulk of the aqueous solution could be useful for the identification of point-source or heterogeneous aqueous analytes, a task that is still a major challenge.[31]

3.3. Near-Continuous Detection of Visible Aqueous Analytes. When monitoring aqueous analytes, the capacity for near-continuous detection is desirable; however, currently it can be complex and tedious.[32] To evaluate our sensor's near-continuous operational capabilities, we tested the system by slowly adding methylene blue dye with a concentration of 0.1 mg/mL into a Petri dish with clean water followed by flushing the system with clean water, all over 1,000 s, as shown in Figure 3. To show the stability of the clean water signal, clean water was dispensed through the inlet stream for an additional 500 s. Methylene blue was chosen due to its environmental relevance.[33−35] A schematic of the overall setup of the experiment is shown in Figure 3a. The methylene blue dye entered the Petri dish on the right and was mixed with a stir bar at a low stir rate before the liquid exited on the left. As the

https://doi.org/10.1021/acs.iecr.4c02774
Ind. Eng. Chem. Res. 2025, 64, 382−391

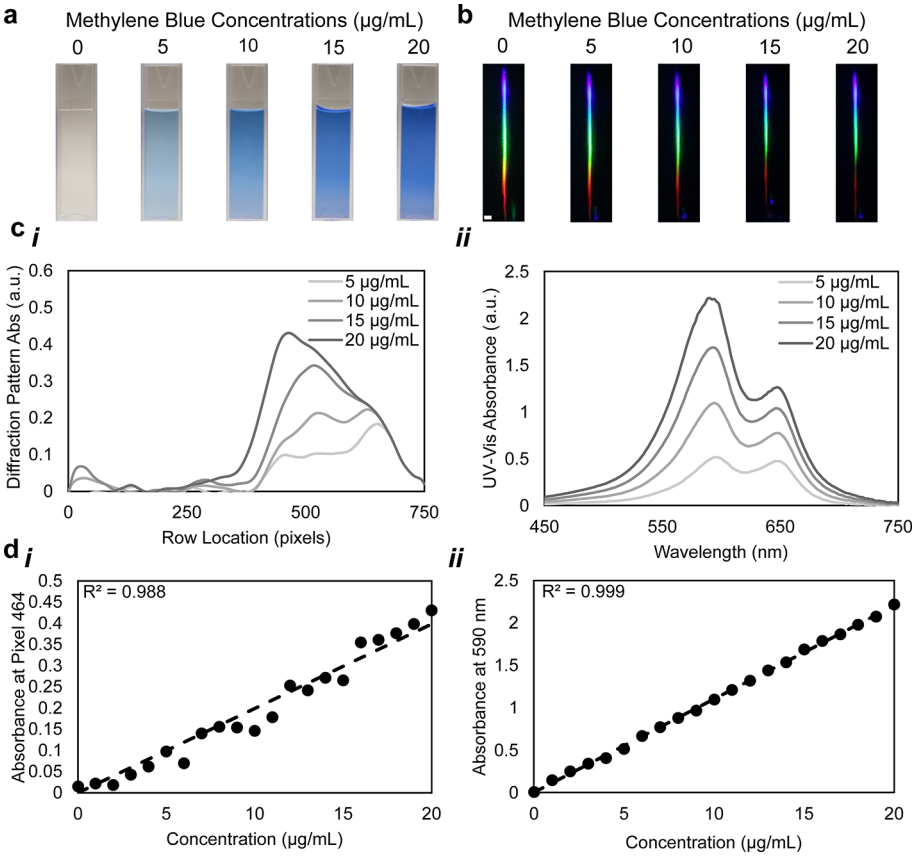

Figure 4. (a) Representative images of the water with experimental concentrations of methylene blue. (b) Representative images of the diffraction pattern with an experimental concentration of methylene blue. Scale bar 1 mm. (c) Spectra of methylene blue at various concentrations in water (*i*) calculated from the diffraction surface sensor and (*ii*) measured using a UV−vis spectrophotometer. (d) Standard curve of blue methylene blue (*i*) calculated from the diffraction sensor and (*ii*) calculated from the UV−vis spectrophotometer.

methylene blue dye entered the Petri dish, the dye mixed with the originally clean water contained in the Petri dish, diluting the overall concentration of methylene blue. During the initial few seconds of the experiment, clean water exited the Petri dish, as the methylene blue dye mixture had not reached the outlet port. Due to the mixing within the Petri dish, the methylene blue dye was more concentrated at the inlet port, which resulted in plumes throughout the dish. Figure 3b displays the evolving color of water over the course of the experiment. The water predominantly appears blue at the 120 s time point and gradually transitions to a colorless state by 1000 s. Figure 3c shows the diffraction pattern at the respective times throughout the near-continuous water quality measurement. During the initial stages, the diffraction pattern appears uniform in intensity and encompasses the full spectrum of colors. The loss of intensity in red, yellow, and green regions of the diffraction pattern, evident in the representative image of 120 s, can be attributed to the absorption of corresponding wavelengths by the chemical molecules in methylene blue dye. Upon the successful clearing out of the methylene blue dye, the diffraction pattern regains its initial full-spectrum diffraction pattern and intensity, as shown in Figure 3c. The calculated maximum absorbance of the diffraction pattern between 0 and 1500 s is shown in Figure 3d. As the methylene blue dye is introduced into the sensor system, the absorbance value steadily increases, until it reaches a plateau at approximately 0.52 au. The plateau is likely due to the diffraction sensor's absorption range limits. As clean water is reintroduced into the system, the absorbance value steadily decreases, ultimately settling at the baseline absorbance level. This shows the diffraction sensor's ability to monitor fluctuations in visible-light-absorbing aqueous analyte levels and its capacity to return to the baseline value. It is important to note that some variability in the baseline absorbance readings could arise from data processing and image acquisition techniques. Further reduction in noise levels might be achieved through the adoption of higher image bit depths, such as 16- or 32-bit images or using RAW image capture.

3.4. Comparison between the Diffraction Sensor System and a Standard UV−vis Absorbance Spectrophotometer. To gain deeper insights into the efficacy of the diffraction sensor system in detecting visible spectrum absorption, we tested increasing concentrations of methylene blue dye with the diffraction sensor and a UV−vis spectrophotometer, as shown in Figure 4. In these tests, the dye solution of 1 μg/mL was added incrementally to increase a final homogeneous concentration of the 20 μg/mL. The images were then converted to gray scale in ImageJ, then the gray value intensities were calculated to absorbance and fit to a curve via Lowess Smoothing using GraphPad Prism 10. Representative images of the changing color of water at increasing dye concentrations are shown in Figure 4a. The corresponding diffraction patterns are shown in Figure 4b, where the intensities of the red, yellow, and green segments progressively diminish as these wavelengths are increasingly

https://doi.org/10.1021/acs.iecr.4c02774
Ind. Eng. Chem. Res. 2025, 64, 382−391

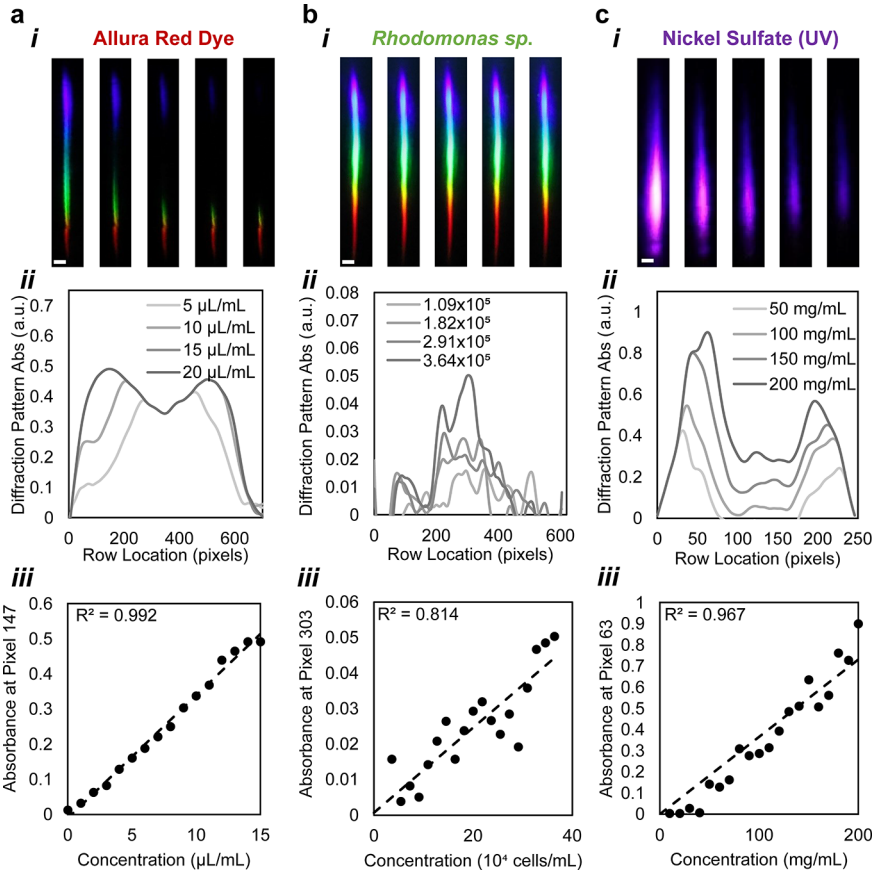

Figure 5. Absorbance from the diffraction surface sensor of different aqueous analytes (a) Allura Red dye (*i*) representative images of the diffraction pattern, (*ii*) diffraction sensor spectra of various concentrations, and (*iii*) the calculated concentration curve. Scale bar = 5 mm. (b) *Rhodomonas sp*. (i) representative images of the diffraction pattern, (*ii*) diffraction sensor spectra of various concentrations and (*iii*) the calculated concentration curve. Scale bar = 5 mm. (c) Nickel sulfate (*i*) representative images of the diffraction pattern, (*ii*) diffraction sensor spectra of various concentrations, and (*iii*) the calculated concentration curve. Scale bar = 10 mm.

absorbed. Figure 4c shows the absorption spectra obtained from both the diffraction pattern (*i*) and the UV−vis spectrophotometer for comparison (*ii*). The spectra of the diffraction surface resemble those obtained from the UV−vis spectrophotometer, suggesting the potential for extracting spectral information through the diffraction sensor. Although the diffraction sensor measures with the corresponding pixel location on the diffraction pattern whereas the commercial UV−vis spectrophotometer measures with corresponding wavelengths, it could be approximated that 0−200 pixels are approximately 450−495 nm and pixels between 600 and 750 are approximately 620−750 nm. Notably, there is a slight shift in the spectral peak from the diffraction sensor, which might be attributed to the sensitivity in the diffraction pattern with any slight changes in the light and camera angle. The slight shift in the spectral peak could result in a lower limit of detection and the accuracy of the diffraction sensor. Standard curves acquired from the diffraction pattern and the spectrophotometer are presented in Figure 4d, with the R^2 value from the diffraction sensor calculated as 0.988 and the UV−vis spectrophotometer as 0.999. It is notable that the R^2 values of the diffraction sensor are close to those obtained from the UV−vis spectrophotometer, despite the UV−vis spectrophotometer having a higher level of complexity. We anticipate that enhancing the signal-to-noise ratio of the diffraction sensor through higher bit depths or using RAW image capture could yield improvements in the R^2 value from the diffraction sensor. Improvements could also increase the absorbance range of the diffraction sensor to be more comparable to commercial UV−vis spectrophotometers. Importantly, the limit of detection of methylene blue dye using the image analysis method described above was calculated to be 5 μg/mL,[36] which is equal to the accepted threshold set by the United States Environmental Protection Agency.[37] The reproducibility was also calculated at the limit of detection value and yielded a relative standard deviation of 45.9%, concentration variance of 0.005 μg/mL, and concentration linearity residual error of 0.01 au.

3.5. Detection of Other Visible Aqueous Analytes.

Since the diffraction sensor detected methylene blue dye and produced spectra similar to a commercial UV−vis spectrophotometer, we tested the ability of the diffraction sensor to produce unique spectra with different aqueous analytes that absorb in either the visible or ultraviolet region of the electromagnetic spectrum, as shown in Figure 5. The Allura Red dye was added to the system in increments of 1 μg/mL until a maximum concentration of 15 μg/mL was achieved. The diffraction pattern was imaged, and its absorbance was calculated as described above. The diffraction pattern, absorption spectrum, and corresponding concentration curve of Allura Red dye are shown in Figure 5a. The absorbance curve increases with increasing concentration, as expected.[38] The Allura Red dye shows two peaks with maximum absorbances at pixels 147 and 479, with the peak at pixel 147 increasing linearly with concentration (R^2 = 0.992). The

https://doi.org/10.1021/acs.iecr.4c02774
Ind. Eng. Chem. Res. 2025, 64, 382−391

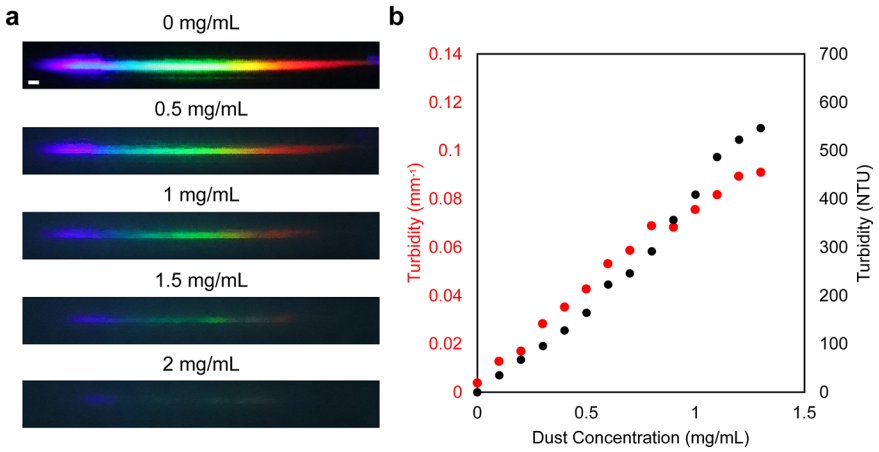

Figure 6. (a) Representative images of A2 fine test dust at increasing concentrations. Scale bar = 1 mm. (b) Calculated turbidity and measured turbidity at increasing concentrations: measurements with the diffraction sensor (left-hand axis, red) and a turbidity meter (right-hand axis, black).

UV−vis of the Allura Red dye has only one peak with a maximum at 498 nm. The difference in spectra between the methylene blue dye, as shown above, and the Allura Red dye shows the diffraction pattern's ability to yield unique spectra for homogeneous mixtures. Additionally, a 50/50 mixture of red and blue dyes was measured to see the effect of multiple analytes in an aqueous solution. Figure S2 shows the spectra for 5 μL of red dye, 5 μL of blue dye, and a 50/50 mixture of the red and blue dye. The 50/50 mixture spectra shows the additive spectra with the absorbance from the red dye and blue dye contributing. Additive spectra is commonly seen in UV−vis spectrophotometry and multiple groups are working to improve the analysis of mixtures.[8,39,40]

As the diffraction sensor performed well in homogeneous aqueous analytes (methylene blue and Allura Red dye), we also tested the sensor's ability to detect aqueous analytes that are often heterogeneous in nature. *Rhodomonas sp.*, a type of microalga with cell sizes between 10 and 15 μm (Figure S3), was selected due to its importance in aquaculture and its production of the red pigment phycoerythrin.[41] Figure 5b*i* shows the representative diffraction patterns corresponding to increasing *Rhodomonas* concentrations in filtered seawater. The measured absorbance spectra of the increasing concentrations are shown in Figure 5b*ii*. Despite the diffraction patterns not showing any differences visible by eye, there is a linear increase of absorbances with increasing concentrations of *Rhodomonas* with an R^2 value of 0.814. The linear correlation may be below desirable values due to the nonuniform distribution of cells within the liquid medium, as expected in biological samples. The highest absorbance is shown in the red region of the diffraction pattern, which is as expected since *Rhodomonas* has a peak absorbance around 650 nm.[42] Other species of microalgae, particularly *Gephyrocapsa huxleyi*, *Chlorella sp.*, and *Synechococcus sp.*, were also tested. The results in Figure S4 show the ability of the sensor system to produce unique spectra for each.

For detection of the ultraviolet-absorbing aqueous analytes, the system was adapted by using an ultraviolet LED, replacing the previously used white LED. Nickel sulfate was added to Milli-Q water in increments of 10 mg/mL until the maximum concentration of 200 mg/mL was achieved. Images of the diffraction pattern were taken between every increase in concentration, the images were analyzed, and absorbance was calculated, as described above. Nickel sulfate was chosen as an aqueous analyte due to its known toxicity as a water contaminant that can result in serious harm to both humans and the environment.[43,44] In water, this compound absorbs light at 400 nm (Figure S5). Figure 5c shows the diffraction pattern, absorption of nickel sulfate, and its calculated concentration curve. As with the aqueous analytes tested that absorbed visible wavelengths, the absorbance increases as the concentration of nickel sulfate increases. The diffraction pattern's intensity decreases with increasing nickel sulfate concentrations, a clear indication of the ultraviolet light absorption by nickel sulfate, as shown in Figure 5c*i*. This is reflected in the calculated spectra shown in Figure 5c*ii*. The concentration curve is shown in Figure 5c*iii*, which has a linear relationship with an R^2 value of 0.967. These results suggest the diffraction sensor's capacity to detect the presence of UV-absorbing aqueous analytes within the tested concentration ranges.

Although it is possible to visually detect the changes by the color of the water due to the analytes tested in some of our experiments, the diffraction pattern provides more information that could be gathered from a simple light and optical sensor. As shown in Figure 5, the diffraction pattern allows for information to be gathered from both the presence and absence of particular colors as well as the overall grayscale values. Effectively, our diffraction sensor enables a UV−vis absorption measurement, providing a unique spectrum for each aqueous analyte and allowing for differentiation between chemicals, as shown in Figure 5.

3.6. Turbidity Information from Particle Scattering.

To determine information gathered from the diffraction sensor of scattered light caused by suspended solids in water,[48] we suspended A2 fine test dust particles in water and imaged with the sensor system. The same image analysis method used to analyze the dye aqueous analytes was applied to these samples, and the absorbance was calculated and converted to a turbidity measurement. Representative images captured of the diffraction pattern are shown in Figure 6a. Here, a reduction in the diffraction pattern's intensity is accompanied by an increase in the overall background of the diffraction sensor, attributed to Mie scattering.[45] Figure 6b shows the calculated turbidity of the A2 fine test dust at increasing concentrations. The diffraction pattern captured above the concentration of 1.6 mg/mL was too high to be quantified by the image analysis software; therefore, analysis was conducted only at values

https://doi.org/10.1021/acs.iecr.4c02774
Ind. Eng. Chem. Res. 2025, 64, 382−391

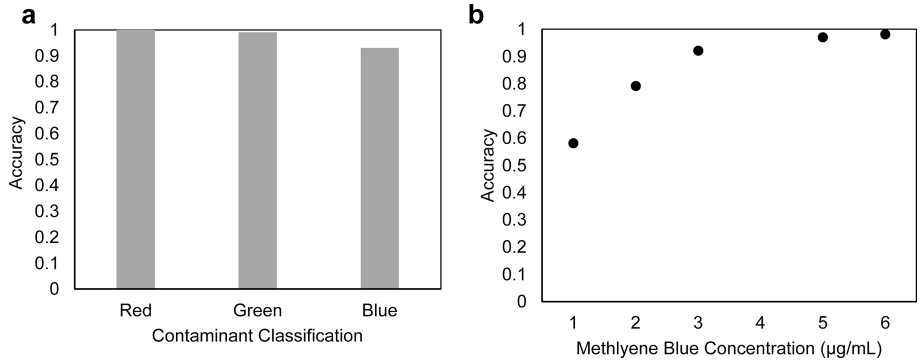

Figure 7. (a) Accuracy of the machine learning algorithm with different aqueous analytes. (b) Accuracy of the machine learning algorithm with different concentrations of methylene blue.

below this concentration. The calculated turbidity values of the sample were compared to the performance of a commercial turbidimeter, as shown in Figure 6b. However, it is important to note that the two different turbidity measurements cannot be directly compared, as the physics of the turbidity measurements are different. In the diffraction pattern sensor, the detector was above the sample, where the full spectrum white light travels through the aqueous solution, diffracts off the diffraction surface, and travels back through the aqueous solution, and its signal is recorded with an image. In the turbidimeter measurements, the light is between 830 and 890 nm and the light travels through the aqueous solution and the detector measures the light scattered 90° from the light path.[46] In these experiments, high levels of turbidity were measured as it is known that fish are significantly affected by turbidities between 10 and 100,000 NTUs, within the range of these measurements.[46] Improvements in the analysis of the diffraction pattern such as noise reduction or color analysis could permit the detection of lower levels of turbidity with this sensor system.

3.7. Employing Machine Learning Image Classification to Enhance and Automate Aqueous Analyte Detection. To assess the potential of automating the readout of the sensor system, we trained a machine learning algorithm to accurately detect and correctly classify differences in the diffraction patterns with different contaminants. A ResNet 34 algorithm was used as it is pretrained with colored images,[47] making it easier for the model to be trained with the diffraction pattern images. We tested the algorithm with three colored dyes: Allura Red, Fast Green, and Brillant Blue. The trained model was then tested with images of the diffraction pattern with either 'clean' water or water with Allura Red, Fast Green, and Brilliant Blue dye labeled as 'red,' 'green,' and 'blue.' Figure 7a shows the accuracy of the machine learning model with different aqueous analytes. The red, blue, and green aqueous analytes have 1, 0.93, and 0.99 accuracy, respectively. This demonstrates that the machine learning algorithm can be used to automate analysis of the diffraction pattern to differentiate the aqueous analytes present from "clean" water with high accuracy levels.

Next, we tested whether the ResNet 34 model could improve the limit of detection of the sensor system beyond what could be achieved with the manual analysis used in Figures 4 and 5 (5 μL/mL). The model was trained using images of methylene blue from 1−6 μg/mL. The results of the subsequent model testing are shown in Figure 7b. The model had an increasing accuracy of 0.58−0.98 with increasing concentrations of methylene blue. The detection limit was calculated based on the concentration above an accuracy of 0.9, the accuracy threshold considered "excellent" for algorithms.[48] The detection limit of the machine learning algorithm was 3 μg/mL, which is lower than the calculated detection limit with the manual image analysis. This is expected as machine learning image classification algorithms have shown to be excellent at detecting differences in images[49,50] and points to the potential of leveraging algorithms for rapid and automated analysis of the sensor data.

4. CONCLUSIONS

Our results show that a low-cost, mass-manufactured diffraction sensor can detect various chemical and biological analytes and can be used to measure analytes in flowing water. The system can also scan the bulk of a liquid volume by changing the location or angle of incidence of the light source. The system can provide information comparable to that of commercial UV−vis spectrophotometers and turbidimeters. In measurements of methylene blue, the diffraction sensor accurately detected concentrations between 5 and 20 μg/mL (R^2 = 0.988), with a limit of detection of 5 μg/mL when using manual analysis and 3 μg/mL when classified with a machine learning algorithm. Additionally, the sensor was able to quantify turbidity comparable to that of a commercial turbidimeter. The sensor could also provide absorbance information for water samples containing microalgae with a concentration of 1.09×10^5 cells/mL. Moreover, the results suggest that the diffraction surface sensor could potentially be useful in creating a new class of mass-deployable, low-cost, near-continuous water sensors.

■ ASSOCIATED CONTENT

Supporting Information

The Supporting Information is available in attached pdf. The Supporting Information is available free of charge at https://pubs.acs.org/doi/10.1021/acs.iecr.4c02774.

Expanded materials and methods, biological sample preparation, microalgae microscopy, refractive index calculation, refractive index, calculated absorbance of dyes, *Rhodomonas sp.* microscopy images, diffraction sensor results of microalgae species, and measured UV−vis spectra of nickel sulfate (PDF)

https://doi.org/10.1021/acs.iecr.4c02774
Ind. Eng. Chem. Res. 2025, 64, 382−391

AUTHOR INFORMATION

Corresponding Author

Caitlin Howell − *Department of Chemical and Biomedical Engineering and Graduate School of Biomedical Science and Engineering, University of Maine, Orono, Maine 04469, United States;* orcid.org/0000-0002-9345-6642; Email: caitlin.howell@maine.edu

Authors

Liza R. White − *Department of Chemical and Biomedical Engineering and Graduate School of Biomedical Science and Engineering, University of Maine, Orono, Maine 04469, United States;* orcid.org/0009-0008-7130-8789

Jordan N. Miner − *Department of Chemical and Biomedical Engineering and Graduate School of Biomedical Science and Engineering, University of Maine, Orono, Maine 04469, United States;* orcid.org/0000-0003-2998-3330

Luke D. McKinney − *Intermedia Graduate School, University of Maine, Orono, Maine 04469, United States*

Lindsay E. Pierce − *Department of Chemical and Biomedical Engineering, University of Maine, Orono, Maine 04469, United States*

Anna Folley − *Department of Chemical and Biomedical Engineering, University of Maine, Orono, Maine 04469, United States*

Ariel Larrabee − *Department of Chemical and Biomedical Engineering, University of Maine, Orono, Maine 04469, United States*

Lea Scrapchansky − *Department of Chemical and Biomedical Engineering, University of Maine, Orono, Maine 04469, United States*

Wyatt Fessler − *Department of Chemical and Biomedical Engineering, University of Maine, Orono, Maine 04469, United States*

Manisha Choudhary − *Department of Civil and Environmental Engineering, University of Maine, Orono, Maine 04469, United States;* orcid.org/0000-0003-1210-6593

Manoj Kamalanathan − *Bigelow Laboratory for Ocean Sciences, East Boothbay, Maine 04544, United States*

Ramin Pouria − *Department of Mechanical Engineering, University of Maine, Orono, Maine 04469, United States*

Saman Zare − *Department of Mechanical Engineering, University of Maine, Orono, Maine 04469, United States;* orcid.org/0000-0002-1249-8462

Emma Perry − *Electron Microscopy Laboratory, University of Maine, Orono, Maine 04469, United States*

Sheila Edalatpour − *Department of Mechanical Engineering, University of Maine, Orono, Maine 04469, United States;* orcid.org/0000-0002-5796-0630

Onur G. Apul − *Department of Civil and Environmental Engineering, University of Maine, Orono, Maine 04469, United States;* orcid.org/0000-0002-2964-8279

Complete contact information is available at: https://pubs.acs.org/10.1021/acs.iecr.4c02774

Author Contributions

L.R.W. and C.H. were responsible for experimental design and data analysis and wrote and revised the manuscript. L.R.W., C.H., O.G.A., E.P., J.M., S.E., M.K., and M.C. edited the manuscript. L.R.W. and J.N.M. wrote software for image and data analysis. L.R.W., L.D.M., L.E.P., A.F., A.L., L.S., W.F., M.C., M.K., R.P., S.Z., and E.P. performed experiments. C.H. supervised the project. All coauthors have given approval to the final version of the manuscript.

Notes

The authors declare no competing financial interest.

ACKNOWLEDGMENTS

The authors thank Mark Hittie, Bill Tripp, and Brandi Couture of Sappi North America, Inc. The authors also thank Theo Erickson, Ainslie Allen, Oisin Biswas, RJ Perry, Evan Leonard, Sandro Zier, Joshua Hamilton, Jeremy Juybari, Michael Mason, Carl Tripp, and Robert Harrington for technical support and supplies. This work was supported by Maine Space Grant Consortium (SG-22-25), National Science Foundation (PFI-RP #2234150, CBET #1939710, CBET #2029378, OIA #2032482), National Institutes of Health (#R01DK128805), and L.L.Bean PFAS Research Program at the University of Maine. Materials were donated by Sappi North America.

REFERENCES

(1) Mekonnen, M. M.; Hoekstra, A. Y. Four Billion People Facing Severe Water Scarcity. *Sci. Adv.* **2016**, *2* (2), No. e1500323.

(2) *Point Source Pollution*. National Oceanic and Atmospheric Administration. https://oceanservice.noaa.gov/education/tutorial_pollution/03pointsource.html (accessed 2023−11−22).

(3) Ejeian, F.; Etedali, P.; Mansouri-Tehrani, H.-A.; Soozanipour, A.; Low, Z.-X.; Asadnia, M.; Taheri-Kafrani, A.; Razmjou, A. Biosensors for Wastewater Monitoring: A Review. *Biosens. Bioelectron.* **2018**, *118*, 66−79.

(4) Zulkifli, S. N.; Rahim, H. A.; Lau, W.-J. Detection of Contaminants in Water Supply: A Review on State-of-the-Art Monitoring Technologies and Their Applications. *Sens. Actuators B Chem.* **2018**, *255*, 2657−2689.

(5) Chong, S. S.; Aziz, A. R. A.; Harun, S. W. Fibre Optic Sensors for Selected Wastewater Characteristics. *Sensors* **2013**, *13*, 8640−8668.

(6) Adu-Manu, K. S.; Tapparello, C.; Heinzelman, W.; Katsriku, F. A.; Abdulai, J.-D. Water Quality Monitoring Using Wireless Sensor Networks: Current Trends and Future Research Directions. *ACM Trans. Sens. Netw.* **2017**, *13* (1), 1−41.

(7) Mao, S.; Chang, J.; Zhou, G.; Chen, J. Nanomaterial-Enabled Rapid Detection of Water Contaminants. *Small* **2015**, *11* (40), 5336−5359.

(8) Navato, A. P.; Mueller, A. V. Enabling Automatic Detection of Anomalies in Wastewater: A Highly Simplified Approach to Defining "Normal" in Complex Chemical Mixtures. *Front. Water* **2021**, *3*, 1−8.

(9) Storey, M. V.; van der Gaag, B.; Burns, B. P. Advances in On-Line Drinking Water Quality Monitoring and Early Warning Systems. *Water Res.* **2011**, *45* (2), 741−747.

(10) Lellis, B.; Fávaro-Polonio, C. Z.; Pamphile, J. A.; Polonio, J. C. Effects of Textile Dyes on Health and the Environment and Bioremediation Potential of Living Organisms. *Biotechnol. Res. Innov.* **2019**, *3*, 275−290.

(11) *Types of Drinking Water Contaminants*. https://www.epa.gov/ccl/types-drinking-water-contaminants (accessed 2023−11−22).

(12) Tissue, B. M.Ultraviolet and Visible Absorption Spectroscopy. In *Characterization of Materials*; John Wiley & Sons, Ltd, 2012; pp 1−13. .

(13) Peacock, M.; Evans, C. D.; Fenner, N.; Freeman, C.; Gough, R.; Jones, T. G.; Lebron, I. UV-Visible Absorbance Spectroscopy as a Proxy for Peatland Dissolved Organic Carbon (DOC) Quantity and Quality: Considerations on Wavelength and Absorbance Degradation. *Environ. Sci. Process. Impacts* **2014**, *16*, 1445−1461.

(14) Tsoumanis, C. M.; Giokas, D. L.; Vlessidis, A. G. Monitoring and Classification of Wastewater Quality Using Supervised Pattern Recognition Techniques and Deterministic Resolution of Molecular Absorption Spectra Based on Multiwavelength UV Spectra Deconvolution. *Talanta* **2010**, *82* (2), 575−581.

(15) Lepot, M.; Torres, A.; Hofer, T.; Caradot, N.; Gruber, G.; Aubin, J.-B.; Bertrand-Krajewski, J.-L. Calibration of UV/Vis Spectrophotometers: A Review and Comparison of Different Methods to Estimate TSS and Total and Dissolved COD Concentrations in Sewers, WWTPs and Rivers. *Water Res.* **2016**, *101*, 519−534.
(16) Gruber, G.; Bertrand-Krajewski, J.-L.; Beneditis, J.; Hochedlinger, M.; Lettl, W. Practical Aspects, Experiences and Strategies by Using UV/VIS Sensors for Long-Term Sewer Monitoring. *Water Pract. Technol.* **2006**, *1* (1), wpt2006020.
(17) Wu, Z.; Wang, X.; Chen, Y.; Cai, Y.; Deng, J. Assessing River Water Quality Using Water Quality Index in Lake Taihu Basin, China. *Sci. Total Environ.* **2018**, *612*, 914−922.
(18) Vasistha, P.; Ganguly, R. Water Quality Assessment of Natural Lakes and Its Importance: An Overview. *Mater. Today Proc.* **2020**, *32*, 544−552.
(19) Buras, M. P.; Solano Donado, F. Identifying and Estimating the Location of Sources of Industrial Pollution in the Sewage Network. *Sensors* **2021**, *21*, 3426.
(20) Andres, L.; Boateng, K.; Borja-Vega, C.; Thomas, E. A Review of In-Situ and Remote Sensing Technologies to Monitor Water and Sanitation Interventions. *Water* **2018**, *10* (6), 756.
(21) Alam, A. U.; Clyne, D.; Jin, H.; Hu, N.-X.; Deen, M. J. Fully Integrated, Simple, and Low-Cost Electrochemical Sensor Array for in Situ Water Quality Monitoring. *ACS Sens.* **2020**, *5* (2), 412−422.
(22) Yang, X.; Ong, K. G.; Dreschel, W. R.; Zeng, K.; Mungle, C. S.; Grimes, C. A. Design of a Wireless Sensor Network for Long-Term, In-Situ Monitoring of an Aqueous Environment. *Sensors* **2002**, *2* (11), 455−472.
(23) Chen, Y.; Han, D. Water Quality Monitoring in Smart City: A Pilot Project. *Autom. Constr.* **2018**, *89*, 307−316.
(24) Grasse, E. K.; Torcasio, M. H.; Smith, A. W. Teaching UV−Vis Spectroscopy with a 3D-Printable Smartphone Spectrophotometer. *J. Chem. Educ.* **2016**, *6*, 146.
(25) Carter, J. B.; Sarkees, A.; Singh, A.; Bean, E. Evaluation of Low-Cost UV-Vis Spectroscopy for Measuring Nitrate Using Synthetic Water Samples. *J. ASABE* **2023**, *66* (4), 929−941.
(26) Laganovska, K.; Zolotarjovs, A.; Vázquez, M.; Mc Donnell, K.; Liepins, J.; Ben-Yoav, H.; Karitans, V.; Smits, K. Portable Low-Cost Open-Source Wireless Spectrophotometer for Fast and Reliable Measurements. *HardwareX* **2020**, *7*, No. e00108.
(27) Boutiette, A. L.; Toothaker, C.; Corless, B.; Boukaftane, C.; Howell, C. 3D Printing Direct to Industrial Roll-to-Roll Casting for Fast Prototyping of Scalable Microfluidic Systems. *PLoS One* **2020**, *15* (12), No. e0244324.
(28) *Rainbow Coated Fabric*. Sappi Global. https://www.sappi.com/rainbow-coated-fabric (accessed 2022−01−30).
(29) Fan, X.; Zheng, W.; Singh, D. J. Light Scattering and Surface Plasmons on Small Spherical Particles. *Light Sci. Appl.* **2014**, *3*, No. e179.
(30) Acharya, R.Interaction of Waves with Medium. In *Satellite Signal Propagation, Impairments and Mitigation*; Elsevier, 2017; pp 57−86. .
(31) Hambly, A. C.; Henderson, R. K.; Storey, M. V.; Baker, A.; Stuetz, R. M.; Khan, S. J. Fluorescence Monitoring at a Recycled Water Treatment Plant and Associated Dual Distribution System − Implications for Cross-Connection Detection. *Water Res.* **2010**, *44* (18), 5323−5333.
(32) Ho, C. K.; Robinson, A.; Miller, D. R.; Davis, M. J. Overview of Sensors and Needs for Environmental Monitoring. *Sensors* **2005**, *5*, 4−37.
(33) Oladoye, P.; Ajuboye, T.; Omotola, E.; Oyewola, O. Methylene Blue Dye: Toxicity and Potential Elimination Technology from Wastewater. *Results Eng.* **2022**, *16*, No. 100678.
(34) Petzer, A.; Harvey, B. H.; Wegener, G.; Petzer, J. P. Azure B, a Metabolite of Methylene Blue, Is a High-Potency, Reversible Inhibitor of Monoamine Oxidase. *Toxicol. Appl. Pharmacol.* **2012**, *258* (3), 403−409.
(35) Fernández-Pérez, A.; Marbán, G. Visible Light Spectroscopic Analysis of Methylene Blue in Water; What Comes after Dimer? *ACS Omega* **2020**, *5*, 29801−29815.
(36) Armbruster, D. A.; Pry, T. Limit of Blank, Limit of Detection and Limit of Quantitation. *Clin. Biochem. Rev.* **2008**, *29* (Suppl1), S49−S52.
(37) Subchapter 2B - Surface Water and Wetland Standards Sections 0.0100 − 0.0300.
(38) Akash, M. S. H.; Rehman, K.*Essentials of Pharmaceutical Analysis*; Springer Nature:: Singapore, 2020. .
(39) Gao, F.; Zhang, H.; Guo, L.; Garland, M. Application of the BTEM Family of Algorithms to Reconstruct Individual UV−Vis Spectra from Multi-Component Mixtures. *Chemom. Intell. Lab. Syst.* **2009**, *95* (1), 94−100.
(40) Martelo-Vidal, M. J.; Vázquez, M. Application of Artificial Neural Networks Coupled to UV−VIS−NIR Spectroscopy for the Rapid Quantification of Wine Compounds in Aqueous Mixtures. *CyTA - J. Food* **2015**, *13* (1), 32−39.
(41) Oostlander, P. C.; van Houcke, J.; Wijffels, R. H.; Barbosa, M. J. Optimization of Rhodomonas Sp. under Continuous Cultivation for Industrial Applications in Aquaculture. *Algal Res.* **2020**, *47*, No. 101889.
(42) Kaňa, R.; Kotabová, E.; Prasil, O. Presence of Flexible Non-Photochemical Quenching in Cryptophytes (Rhodomonas Salina). *In Advanced Topics in Science and Technology in China* **2013**, 489−492.
(43) Nickel Sulfate, N. K. S., 1999. https://cameochemicals.noaa.gov/chris/NKS.pdf (accessed 2024−07−23).
(44) *Nickel in Drinking-Water*, 2005. https://cdn.who.int/media/docs/default-source/wash-documents/wash-chemicals/nickel-background-document.pdf?sfvrsn=90644b9f_9 (accessed 2023−05−15).
(45) *ISO 12103−1, A2 Fine Test Dust*. Powder Technology Inc.https://www.powdertechnologyinc.com/product/iso-12103-1-a2-fine-test-dust/ (accessed 2023−08−09).
(46) Lloyd, D. S.; Koenings, J. P.; Laperriere, J. D. Effects of Turbidity in Fresh Waters of Alaska. *North Am. J. Fish. Manag.* **1987**, *7* (1), 18−33.
(47) Koonce, B.ResNet 34. In *Convolutional Neural Networks with Swift for Tensorflow: Image Recognition and Dataset Categorization*; Koonce, B., Ed.; Apress: Berkeley, CA, 2021; pp 51−61. .
(48) Bradley, A. P. The Use of the Area under the ROC Curve in the Evaluation of Machine Learning Algorithms. *Pattern Recognit.* **1997**, *30* (7), 1145−1159.
(49) Joy, C.; Sundar, G. N.; Narmadha, D.AI Driven Automatic Detection of Bacterial Contamination in Water: A Review. In *2021 5th International Conference on Intelligent Computing and Control Systems (ICICCS)*; 2021; pp 1281−1285. 10.1109/ICICCS51141.2021.9432171.
(50) Khan, A. A.; Laghari, A. A.; Awan, S. A. Machine Learning in Computer Vision: A Review. *EAI Endorsed Trans. Scalable Inf. Syst.* **2021**, *8* (32), e4−e4.

https://doi.org/10.1021/acs.iecr.4c02774
Ind. Eng. Chem. Res. 2025, 64, 382−391